

PFC/JA-86-28

A HIGH-POWER RADIO-FREQUENCY PLASMA SOURCE

Petty, C. Craig; Smith, Donald K.

May 1986

Plasma Fusion Center
Massachusetts Institute of Technology
Cambridge, Massachusetts 02139 USA

Submitted for publication in: Review of Scientific Instruments.

ABSTRACT

A high-power radio-frequency plasma source was built and tested for an antenna frequency of 2.45 MHz. A puff valve fed hydrogen gas into a plasma chamber made from 4"-diameter Pyrex tubing. A helical antenna was wound directly around this chamber. The plasma source was surrounded by a magnetic bucket which used a longitudinal line-cusp geometry.

For 20 kW of RF input power, the peak electron density was $2.0 \times 10^{19} \text{ m}^{-3}$, the electron temperature was 2.0 eV, the ion temperature was 0.9 eV, and the atomic hydrogen density was $4.4 \times 10^{19} \text{ m}^{-3}$. For 90 kW of RF input power, the peak electron density was $8.9 \times 10^{19} \text{ m}^{-3}$, the electron temperature was 2.5 eV, the ion temperature was 3.0 eV, and the atomic hydrogen density was $2.3 \times 10^{19} \text{ m}^{-3}$. The plasma source had a typical current efficiency of 6 A/kW. A theoretical model for the plasma loading resistance was developed.

INTRODUCTION

A high-power radio-frequency plasma source having no internal parts has been built and tested for an antenna frequency of 2.45 MHz. A detailed description of this plasma source is available¹. Related work on a RF plasma source for neutral beams has been done by DiVergilio et al.² using an internal antenna. In the plasma source described here, power is transferred from an external helical antenna to the plasma via the induced plasma currents. Collisions between electrons and ions give rise to a plasma resistivity through which power is dissipated in the plasma. The power is subsequently thermalized by the rapid electron-electron Coulomb collisions. The electron-electron collision frequency is approximately 70 times the electron bounce frequency in the magnetic cusp fields, 90 times the electron-neutral collision frequency, and 200 times the applied antenna frequency. The electrons therefore absorb the RF energy through a random walk process.

This plasma source potentially has many uses. First, it could be used as a source of low-energy hydrogen atoms for refueling a plasma machine. The large amount of Frank-Condon neutrals produced (620 A at 20 kW of RF power) suggests that it could be used for the start-up phase of a tandem mirror. A second use would be as an ion source for neutral beams, where a small but intense RF plasma source could illuminate a larger grid set. A RF plasma source could also serve as a low-energy high-current ion and neutral source for the etching of semiconductors. Finally, preliminary experiments have begun on using the RF plasma source as a high-current plasma switch.

I. PLASMA SOURCE DESIGN

The plasma chamber consisted of a cylindrical Pyrex cap-piece, 4" in diameter and 7" long. Pyrex was chosen because it has a low hydrogen-atom recombination coefficient³ which allowed a high H^0 flux. A hole was bored in the center of the enclosed end, and a glass tube was attached to allow hydrogen gas to be puffed directly into the plasma. The open end of the Pyrex cap was connected to a pumping chamber by a Pyrex cross-piece (see Figure 1). One of the perpendicular openings in the cross-piece was used as a port for two Langmuir probes.

A helical antenna was directly wound around the Pyrex plasma chamber. The antenna had eleven turns spaced 0.5" apart. The antenna matching network is shown in Figure 2. The helical antenna acted as an inductor. Two 1000 pF capacitors connected both ends of the antenna to ground. This formed a LC resonant loop at 2.45 MHz which allowed a large amount of circulating energy. A 1000 pF variable capacitor was used to match the 50 Ω transmission line to the resonant loop. As the plasma density increased, the amount of capacitance needed to perform this match also increased. The vacuum Q of the resonant loop was 61.

During a plasma shot, the natural plasma diamagnetism tended to lower the effective inductance of the antenna. If no adjustment was made, this would have taken the circuit away from its resonant point. Therefore a 10 pF variable capacitor was added in parallel with each 1000 pF fixed capacitor. This allowed the total resonating capacitance to be increased to offset the decrease in the antenna inductance.

A magnetic bucket surrounded the plasma chamber and antenna. Eight columns of permanent ceramic magnets were used in a longitudinal line-cusp geometry. Each magnet column was covered with a mild steel plate, the

plates forming an octagon to enclose the magnetic lines of flux (see Figure 3). Underneath each magnet column was a mild steel bar with grooves cut in its underside to allow the helical antenna to pass through. Having the antenna inside the magnetic bucket reduced the antenna losses while the mild steel bars allowed the magnetic poles to be brought closer to the plasma. The magnetic field strength at the plasma surface was 0.33 kG. A mild steel endplate completed the longitudinal line-cusp geometry with three additional rows of magnets. A hole was drilled through the center of the endplate to allow the gas feed to pass through.

All of the mild steel components were copper plated .1-.2 mm thick and the magnet columns were wrapped with copper tape to reduce antenna eddy-current losses. In addition, Teflon strips were inserted between the outer mild-steel plates to eliminate circulating currents driven by the antenna. The magnetic bucket was also filled with silicone oil to prevent a corona from forming around the antenna due to air breaking down.

The control system for operating the RF plasma source is shown in Figure 4. Since no provision for cooling the source was made, and due to constraints on the RF transmitter, the plasma source was run using short pulses. Each plasma shot started with a pulse from the source trigger. This trigger pulse went to pulse generator #1 which opened the puff valve for 17 ms. The amount of hydrogen gas released into the plasma chamber was easily varied with a needle valve. An internal delay generator was built into the source trigger which produced a second trigger pulse after a variable delay. This delayed trigger went to pulse generator #2 which fired the RF transmitter. The RF power was typically delayed by 10 ms to allow time for the hydrogen gas to reach the plasma chamber from the puff valve. The RF pulse to the plasma source was 5 ms long.

II. EXPERIMENTAL RESULTS

A. Langmuir probes

Two Langmuir probes were used to measure the ion-saturation current-density, electron density, electron temperature, and plasma potential of the RF plasma source. Langmuir probe #1 was bent in a L-shape (see Figure 1) in order to locate its tip in the plasma source aperture, which was 18.0 cm from the gas feed. Langmuir probe #2 was a straight probe located 20.7 cm behind Langmuir probe #1.

The RF input power was varied from 10 to 100 kW, and the gas feed rate was varied from 150 to 3840 equivalent amps of H. The peak electron density vs. RF power at Langmuir probe #1 is shown in Figure 5 for various hydrogen feed-rates. The ion-saturation current-density varied with RF power and hydrogen feed rate like the electron density, with peak values ranging from 0.4 A/cm^2 to 13.5 A/cm^2 . The peak electron temperature vs. RF power at Langmuir probe #1 is shown in Figure 6 for various hydrogen feed-rates. The plasma potential varied with RF power and hydrogen feed rate like the electron temperature, with peak values ranging from 5.3 V to 16.7 V.

Radial profiles of these basic plasma parameters were taken at both Langmuir probes. Figure 7 shows both the electron-density and electron-temperature radial-profiles at Langmuir probe #1 for 20 kW of RF power and a gas feed rate of 1110 A of H. Since the electron temperature profile was flat across the source aperture, the ion-saturation current-density had a radial profile like that of the electron density with a peak value of 2.4 A/cm^2 . The plasma-potential radial-profile was flat across the source aperture with a value of 7.3 V. The electron-density radial-profile was

much broader at Langmuir probe #2 than at Langmuir probe #1, with a peak value of $5.2 \times 10^{17} \text{ m}^{-3}$. The peak ion-saturation current-density had fallen to $.043 \text{ A/cm}^2$. The electron temperature at Langmuir probe #2 was 1.0 eV and the plasma potential was 3.0 V.

Figure 8 shows the electron-density and electron-temperature radial-profiles at Langmuir probe #1 for 90 kW of RF power and a gas feed rate of 1870 A of H. The peak ion-saturation current-density was 11.8 A/cm^2 . The plasma potential again had a similar profile as the electron temperature with a peak value of 8.4 V. The electron-density radial-profile at Langmuir probe #2 was flat across most of the plasma diameter with a value of $7.5 \times 10^{18} \text{ m}^{-3}$. The peak ion-saturation current-density had fallen to 0.47 A/cm^2 . The electron temperature at Langmuir probe #2 had lost its center peak and was 0.5 eV. The plasma potential kept its center peak with a maximum value of 0.8 V.

B. Spectroscopy

A spectrometer was used to measure the ion temperature and streaming atom energy from Doppler broadening. The spectrometer observed the plasma source through a large Plexiglas window on the far end of the vacuum chamber. A lens focused the central region of the plasma onto the spectrometer slit. When a stationary reference source was needed, a hydrogen lamp was placed where it could be viewed by the spectrometer using a beam splitter.

The spectral line was deconvoluted in the following manner for the optically thin plasma. First, it was assumed that the plasma was made up of two separate distributions of atoms: a stationary Maxwellian and a group streaming out of the source. The center wavelength of the Maxwellian was

determined by the reference lamp peak. A symmetric Maxwellian was constructed by reflecting the red end of the spectral line over to the blue side. This Maxwellian was then subtracted from the total spectral line, leaving a final distribution which was taken to be that of atoms streaming out of the source. The difference between the peaks of the two distributions was used to find the average velocity of the streaming atoms.

An example of this spectral line deconvolution is given in Figure 9 for the H_{α} line at 20 kW of RF power and 1110 A of H. This figure indicated a streaming atom energy of 1.8 eV. The H_{β} line gave a streaming atom energy of 1.5 eV, thus supporting this method of deconvolution. For 90 kW of RF power and 1870 A of H, a streaming atom energy of 3.6 eV for the H_{α} line and 4.0 eV for the H_{β} line was found.

The average ion temperature was found from the FWHM of the stationary Maxwellian distribution. The instrumental resolution was 0.35 Å. The H_{α} rather than the H_{β} line was used to measure Doppler broadening because pressure broadening could be neglected for the H_{α} line. The average ion temperature vs. RF power is shown in Figure 10 for various hydrogen feed-rates.

C. Thermistor probe

A thermistor located 85.5 cm from the plasma source aperture was used to measure the radiated light power and atomic-hydrogen current-density, from which the atomic hydrogen density could be inferred. The free standing thermistor observed the plasma through a collimating tube. Two permanent ceramic magnets were placed around the tube to deflect charged particles. This allowed only light and neutral particles to strike the thermistor.

The change in the thermistor resistance was measured using an AC bridge (see Figure 11). A high pass filter was used on the bridge output to filter out ground currents caused by charged particles striking the probe shielding. Before a plasma shot, the bridge was balanced using the variable resistor and capacitor. Immediately after a plasma shot, the change in the thermistor resistance (R_t) caused a non-zero ΔV . This differential signal was used to calculate the rise in the thermistor temperature. Knowing the thermistor heat capacity (experimentally determined using a He-Ne laser), the total amount of energy absorbed by the thermistor could be calculated.

The thermistor measured both light and neutral particle energy. In order to measure light energy alone, a Li-F window was placed in front of the thermistor. This allowed visible and ultraviolet light to pass through but blocked particles. With this data, the light energy could be subtracted from the total energy to leave the neutral particle energy. Since the mean free path for the cold hydrogen gas was typically a few centimeters, the molecular hydrogen density was much less than the atomic hydrogen density. Therefore the neutral particles striking the thermistor were mainly atomic hydrogen.

A time evolution of the thermistor temperature was taken by varying the length of the RF pulse, thus allowing the plasma light power and atomic hydrogen power to be calculated. Assuming that the plasma light was isotropic, the total light power radiated by the plasma was calculated to be 6.3 kW at 20 kW of RF power, and 67 kW at 90 kW of RF power. The atomic-hydrogen current-density could be calculated from the atomic hydrogen power by dividing it by the streaming atom energy. Assuming that the particle beam from the plasma source expanded like a disk source (as suggested by the expansion of the ion-saturation current-density between Langmuir probes

#1 and #2), the atomic-hydrogen current-density at the source aperture was calculated to be 7.7 A/cm^2 for 20 kW of RF power and 1110 A of H, and 5.7 A/cm^2 for 90 kW of RF power and 1870 A of H. From this result, the atomic hydrogen density was estimated to be $4.4 \times 10^{19} \text{ m}^{-3}$ for 20 kW of RF power, and $2.3 \times 10^{19} \text{ m}^{-3}$ for 90 kW of RF power.

D. Plasma source efficiency

The current efficiency was calculated by dividing the total ion current flowing out of the plasma source aperture by the RF input power. The current efficiency initially increased with increasing RF power, but soon saturated at a typical value of 6 A/kW, indicating that approximately 170 eV/ion was needed to sustain the plasma. The gas efficiency was calculated by dividing the total ion current flowing out of the plasma source aperture by the hydrogen feed rate (in equivalent amps of H). The gas efficiency steadily increased with increasing RF power from a low of 7% to a high of 60%. The RF coupling efficiency, given by the ratio of the plasma loading resistance to the total resistance of the resonant loop, was typically 96% and relatively independent of RF power or hydrogen feed rate.

E. Plasma loading resistance

A large plasma loading-resistance is necessary for an efficient RF plasma source. The plasma loading resistance arises from the finite resistivity of the plasma. Free electrons are accelerated by the RF electric fields, their velocity vectors being randomized through collisions with ions and neutral atoms. This leads to ohmic heating of the electrons and ionization of the background gas.

It is important to model the plasma loading resistance in order to optimize the design of future RF plasma sources. Inside the plasma, the RF electric fields fall off exponentially like the skin depth. The plasma current can be modeled as if it were flowing entirely in the first skin depth, thus

$$J = \frac{N I}{\delta}, \quad (1)$$

where N is the number of turns per unit length of the antenna, I is the antenna current, and δ is the skin depth determined from the plasma resistivity. The power dissipated in the plasma through the plasma resistivity (η) is equal to

$$P = \frac{1}{2} \eta J^2 V. \quad (2)$$

Here V is the volume in which the modeled plasma current flows, which is

$$V = 7.8 r \delta L, \quad (3)$$

where r is the plasma radius and L is the antenna length. Modeling the plasma as a simple resistor (R_p) leads to a dissipated power of

$$P = \frac{1}{2} R_p I^2. \quad (4)$$

Setting equation (2) equal to equation (4) gives a theoretical plasma loading-resistance of

$$R_p = 7.8 r L N^2 \left(\pi \mu_o \nu_{rf} \eta \right)^{1/2}, \quad (5)$$

where ν_{rf} is the applied antenna frequency.

The plasma resistivity due to electron-ion collisions is referred to as Spitzer resistivity and is given by⁴

$$\eta_{sp} = 5.2 \times 10^{-5} \ln A T_e^{-3/2}, \quad (6)$$

where T_e is the electron temperature in eV, $\ln A$ is the Coulomb logarithm, and η_{sp} is in Ω -m. A plot of the theoretical plasma loading-resistance from Spitzer resistivity vs. RF power is given in Figure 12 for a gas feed rate of 1570 A of H. The experimental plasma loading-resistance is also

shown. There is some agreement at low powers, but the results rapidly diverge at high powers. Since no microwave radiation was detected at the plasma frequency, this anomalous resistivity of the plasma was not due to a high-frequency plasma instability. Including the resistivity due to electron-neutral collisions gave a substantial correction at low powers which resulted in good agreement between the theoretical and experimental plasma loading-resistance. At high powers, however, the resistivity due to electron-neutral collisions became negligible. Electron-wall collisions may have been responsible for the additional plasma resistivity.

III. DISCUSSION

A comparison of some of the plasma parameters for the RF plasma source and a filament-arc source is shown in Table I. The filament-arc source had dimensions of 38 cm \times 10 cm and did not use a magnetic bucket⁵. There are many advantages to using a RF plasma source rather than a filament-arc source, such as (1) omission of the filaments which limit the lifetime of a filament-arc source, (2) absence of the large sheath drop of an arc discharge which causes sputtering and lowers the power efficiency, (3) eliminating the need for large floating power-supplies, and (4) easier control of the plasma discharge.

ACKNOWLEDGMENTS

We would like to thank Professor Ian Hutchenson for his help in the area of plasma diagnostics, Dr. James Irby and Tom Moran for their assistance in taking and analyzing spectroscopy data, and Douglas Kevan for his

help with the RF transmitter. This work was performed under D.O.E. contract no. DE-AC02-78ET51013. Craig Petty was financially supported by the Magnetic Fusion Energy Technology Fellowship administered by Oak Ridge Associated Universities.

¹C. Petty, A high-power radio-frequency plasma source, SM thesis, Massachusetts Institute of Technology, Dept. of Nuclear Engineering (1986).

²W. DiVergilio, K. Ehlers, V. Fosnight, D. Kippenhan, R. Pyle and M. Vella, J. Vac. Sci. Technol. A **3**, 1218 (1985).

³B. Wood and H. Wise, J. Chem. Phys. **30**, 6 (1958).

⁴L. Spitzer, Physics of fully ionized gases (Interscience, New York 1962).

⁵R. Torti (private communication).

Table I. Comparison of RF and filament-arc sources.

Plasma parameter	RF source	Filament-arc source
Input power	50 kW	50 kW
Gas feed-rate	1870 A of H	450 A of H
Ion current density	7.1 A/cm ²	.18 A/cm ²
Electron density	6.2×10 ¹⁹ m ⁻³	9.5×10 ¹⁷ m ⁻³
Electron temperature	1.8 eV	5.0 eV
Current efficiency	6.2 A/kW	1.4 A/kW
Gas efficiency	16%	15%

Figure 1. Cross-section of vacuum chamber.

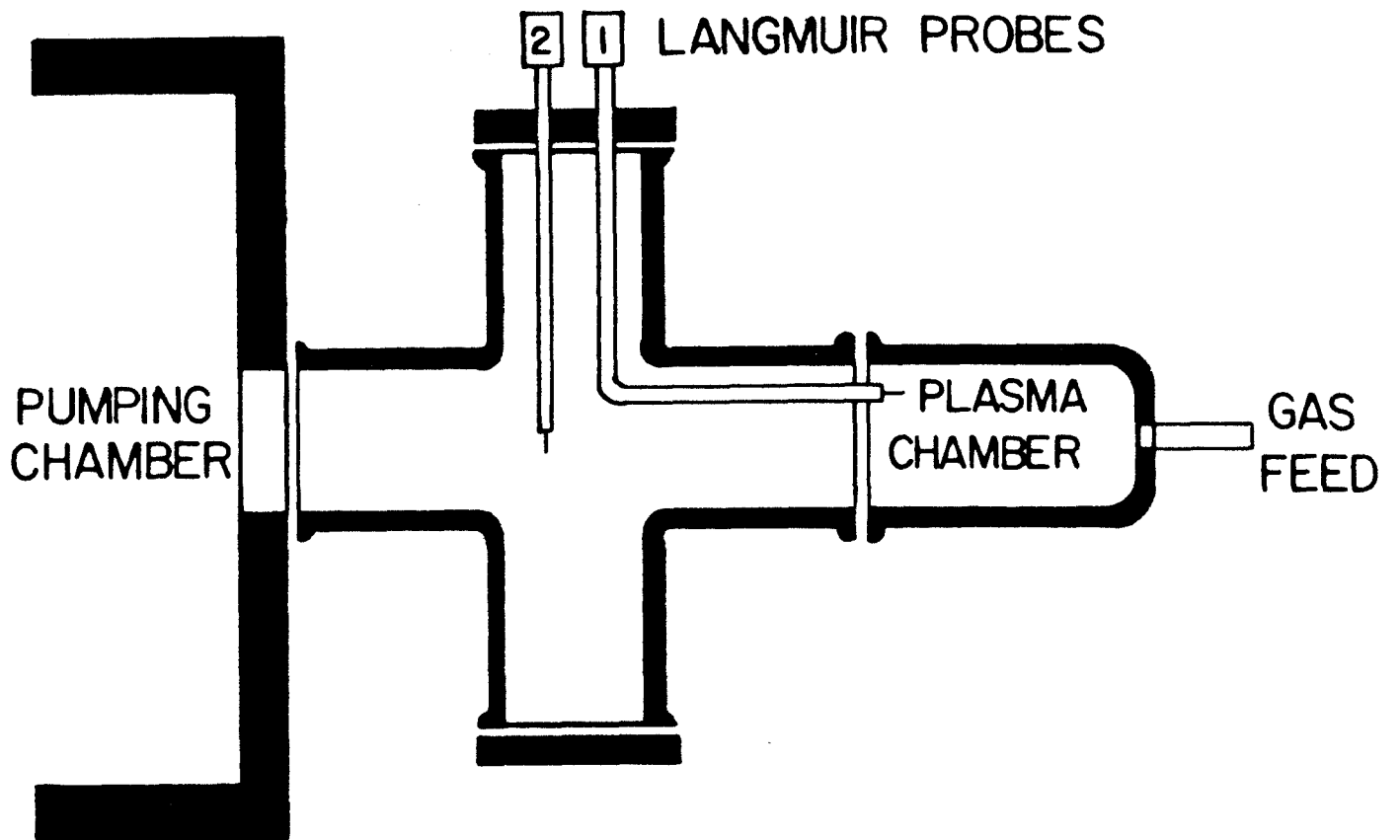


Figure 2. Antenna matching network.

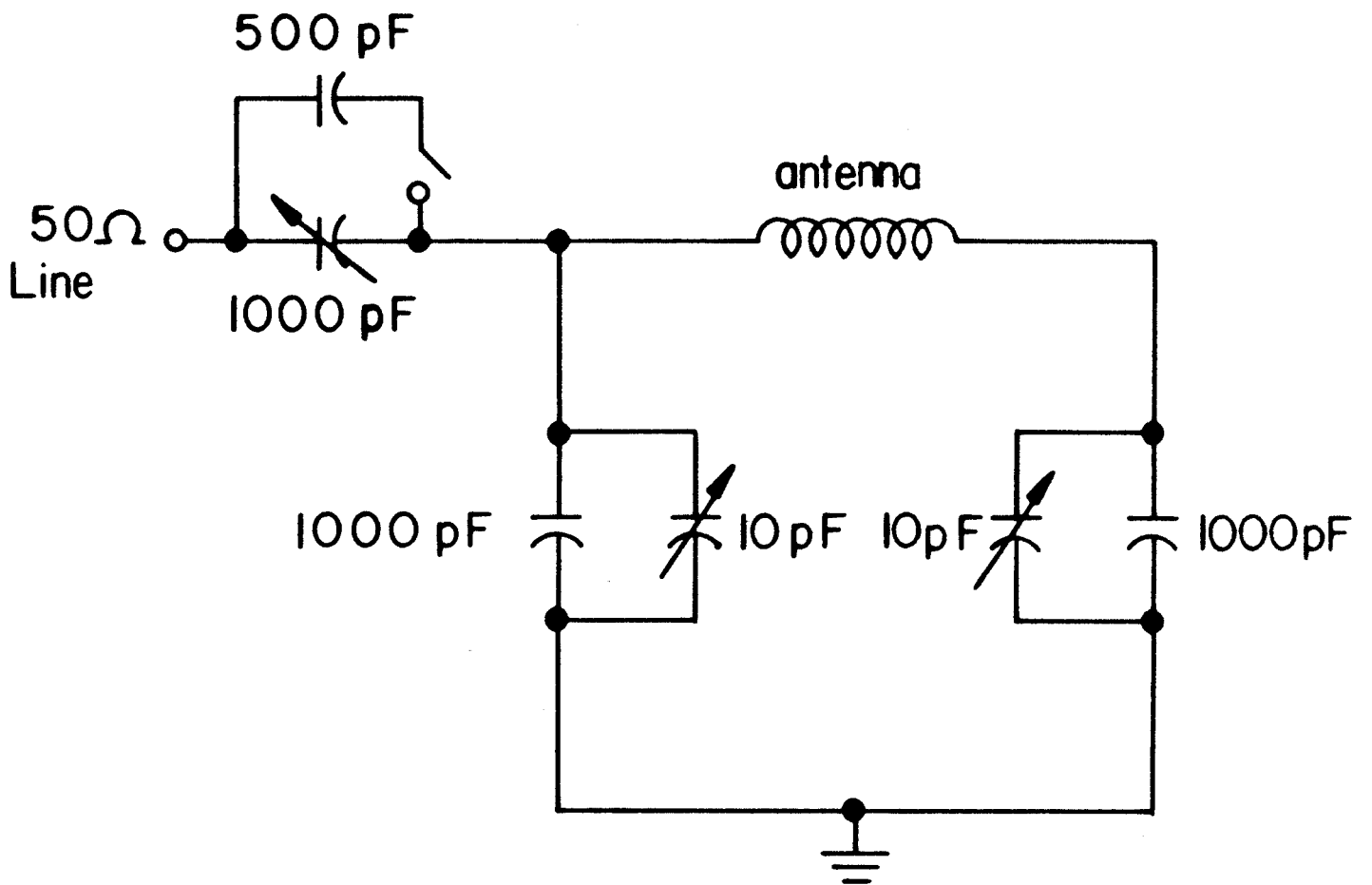


Figure 3. Cross-section of magnetic bucket.

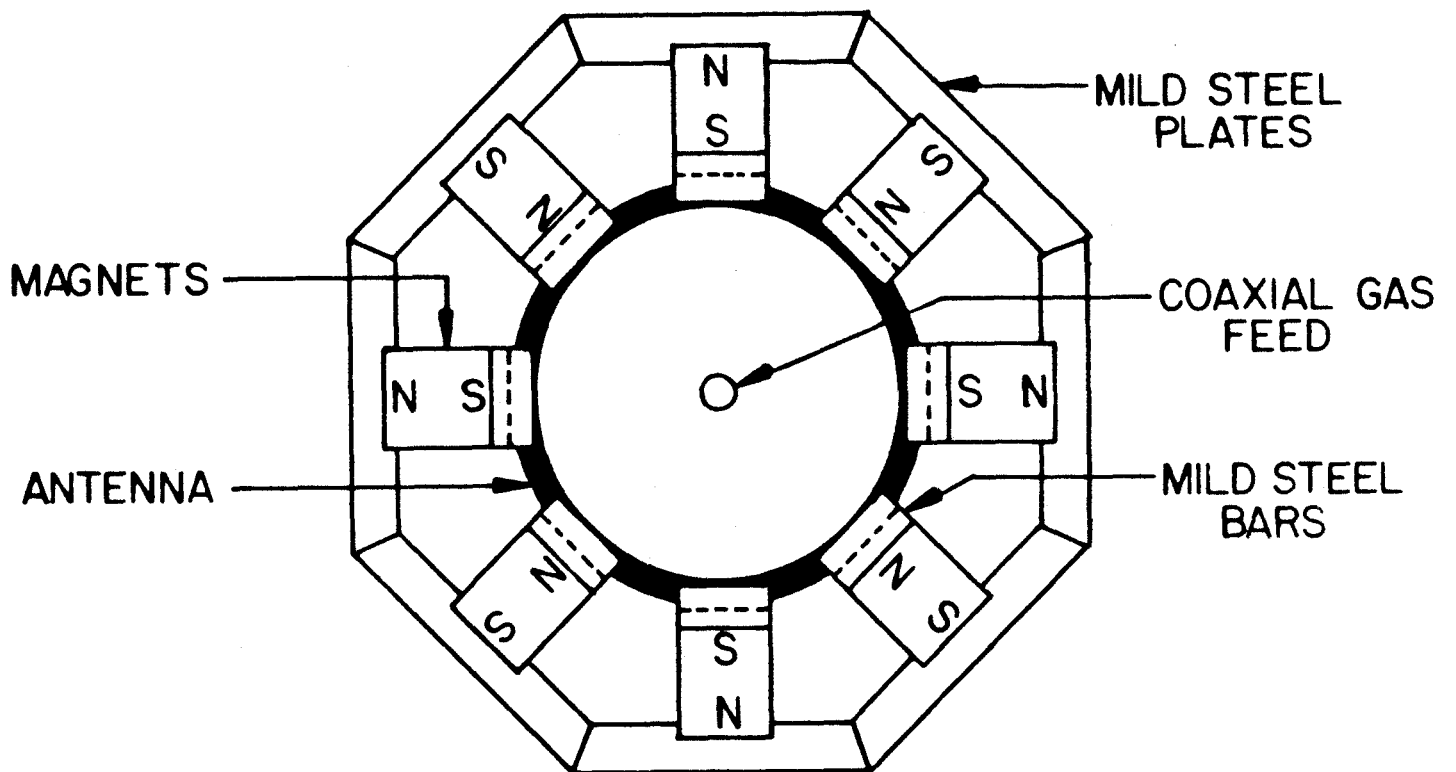


Figure 4. Block diagram of plasma-source control system.

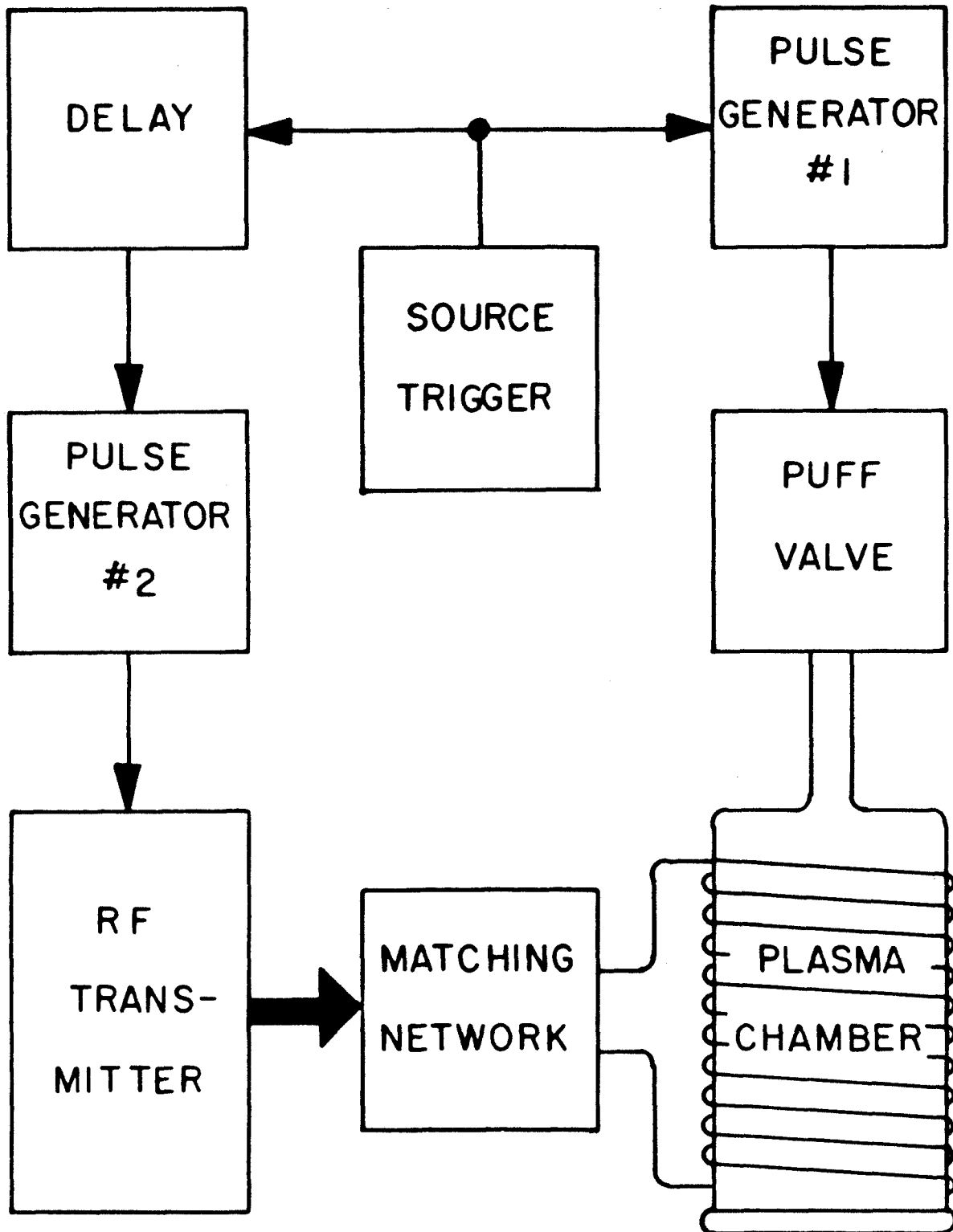


Figure 5. Peak electron density vs. RF power for various hydrogen feed-rates.

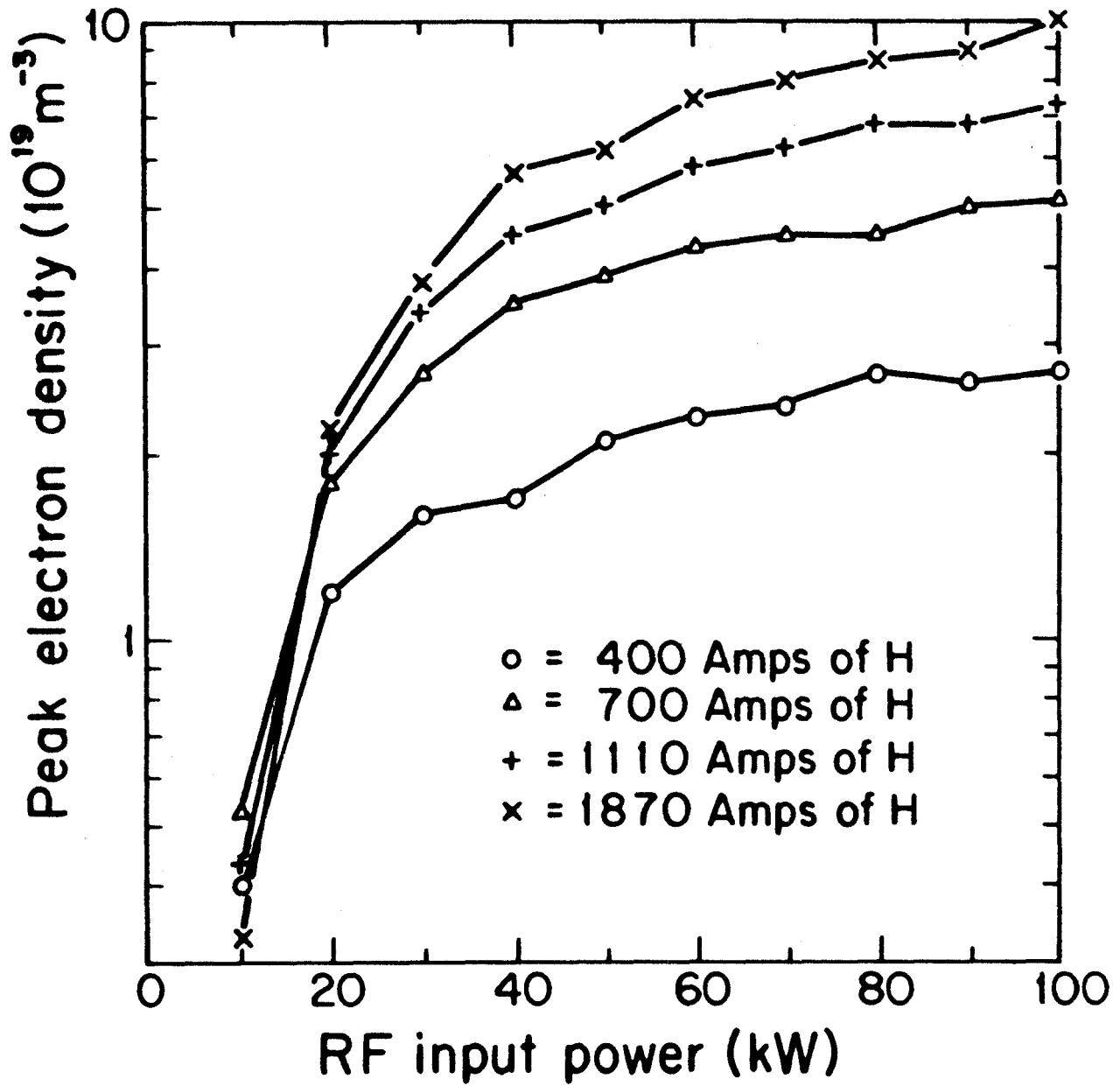


Figure 6. Peak electron temperature vs. RF power for various hydrogen feed-rates.

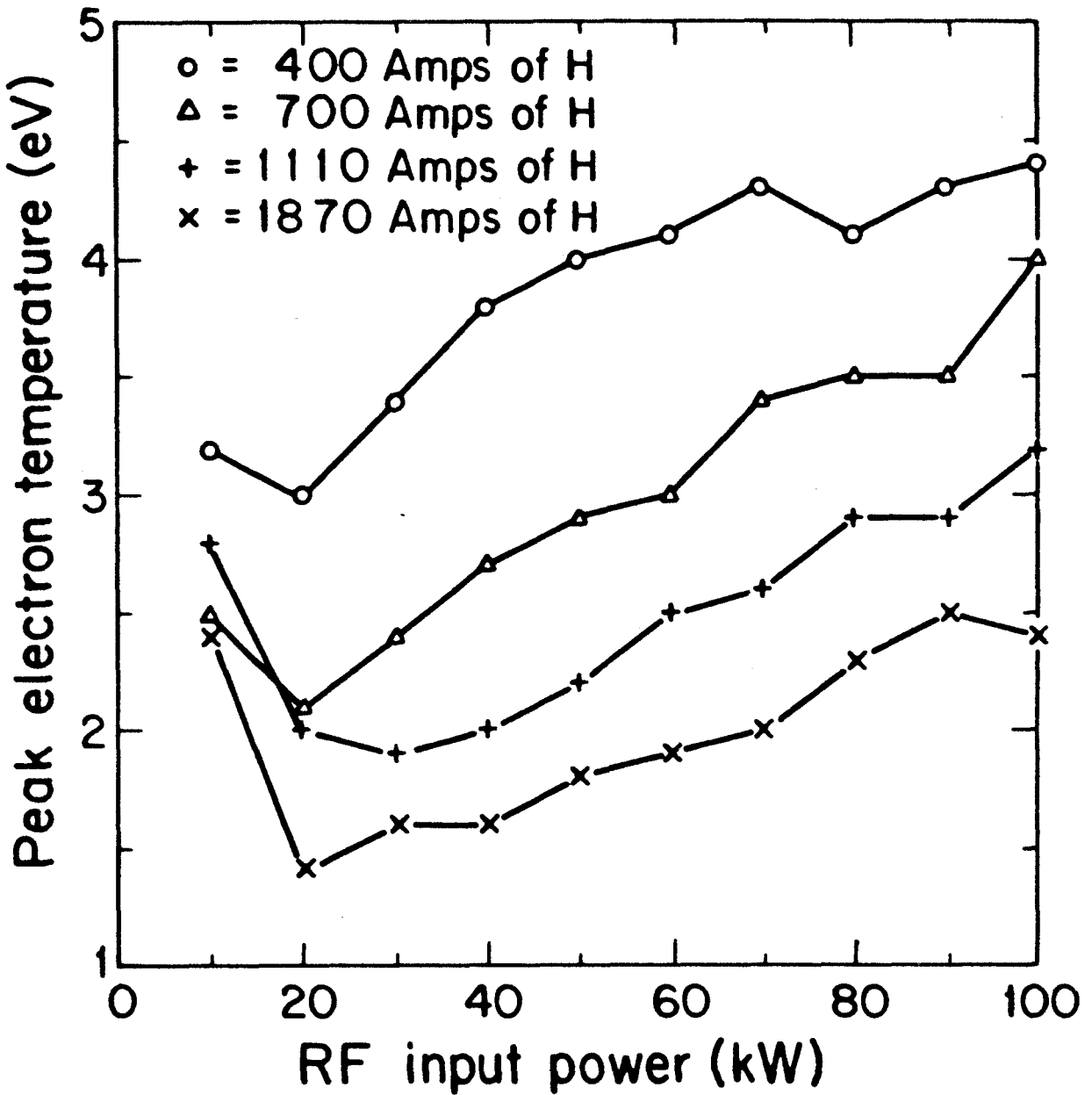


Figure 7. Electron-density and electron-temperature radial-profiles at Langmuir probe #1 for 20 kW of RF power and 1110 A of H.

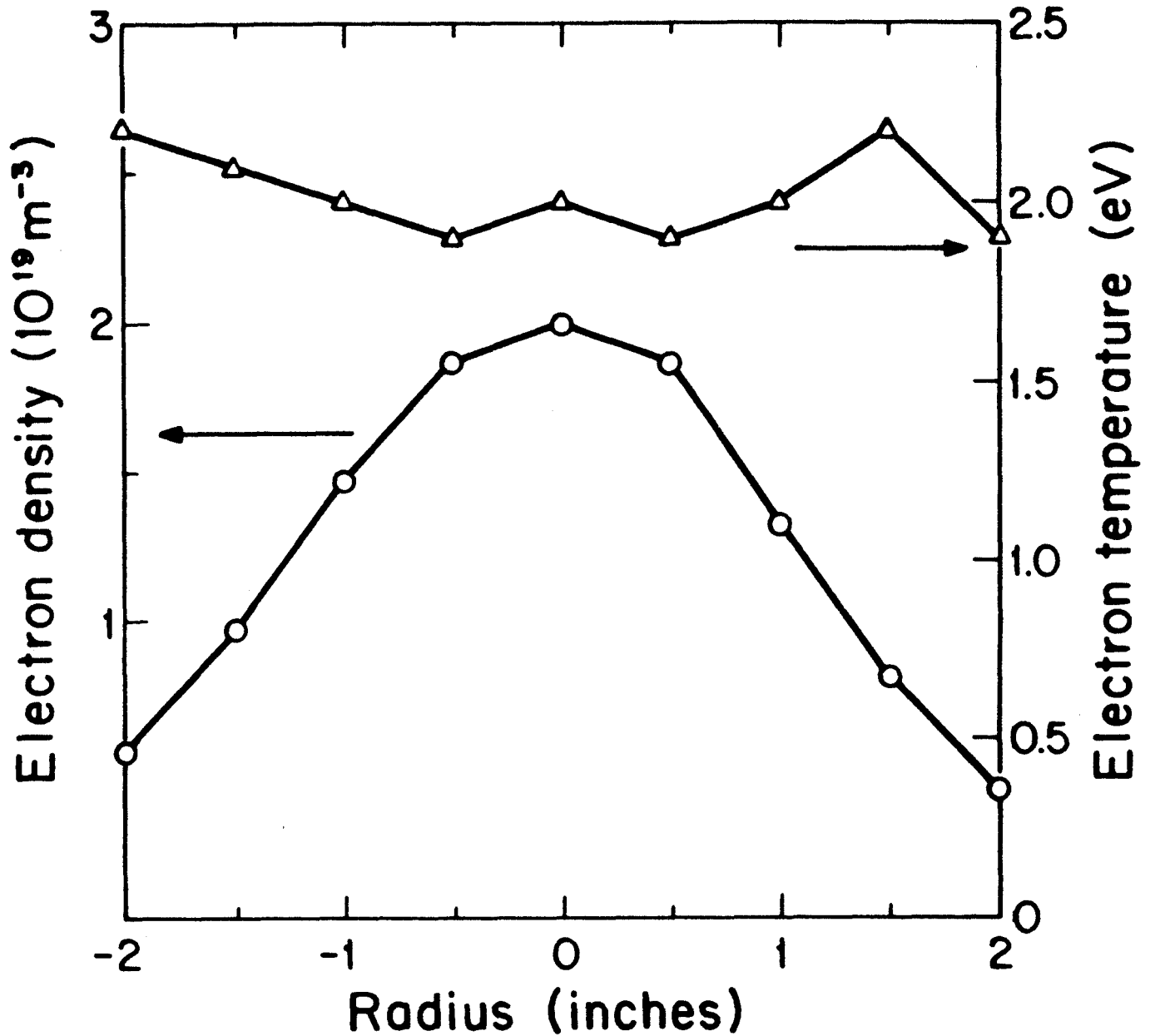


Figure 8. Electron-density and electron-temperature radial-profiles at Langmuir probe #1 for 90 kW of RF power and 1870 A of H.

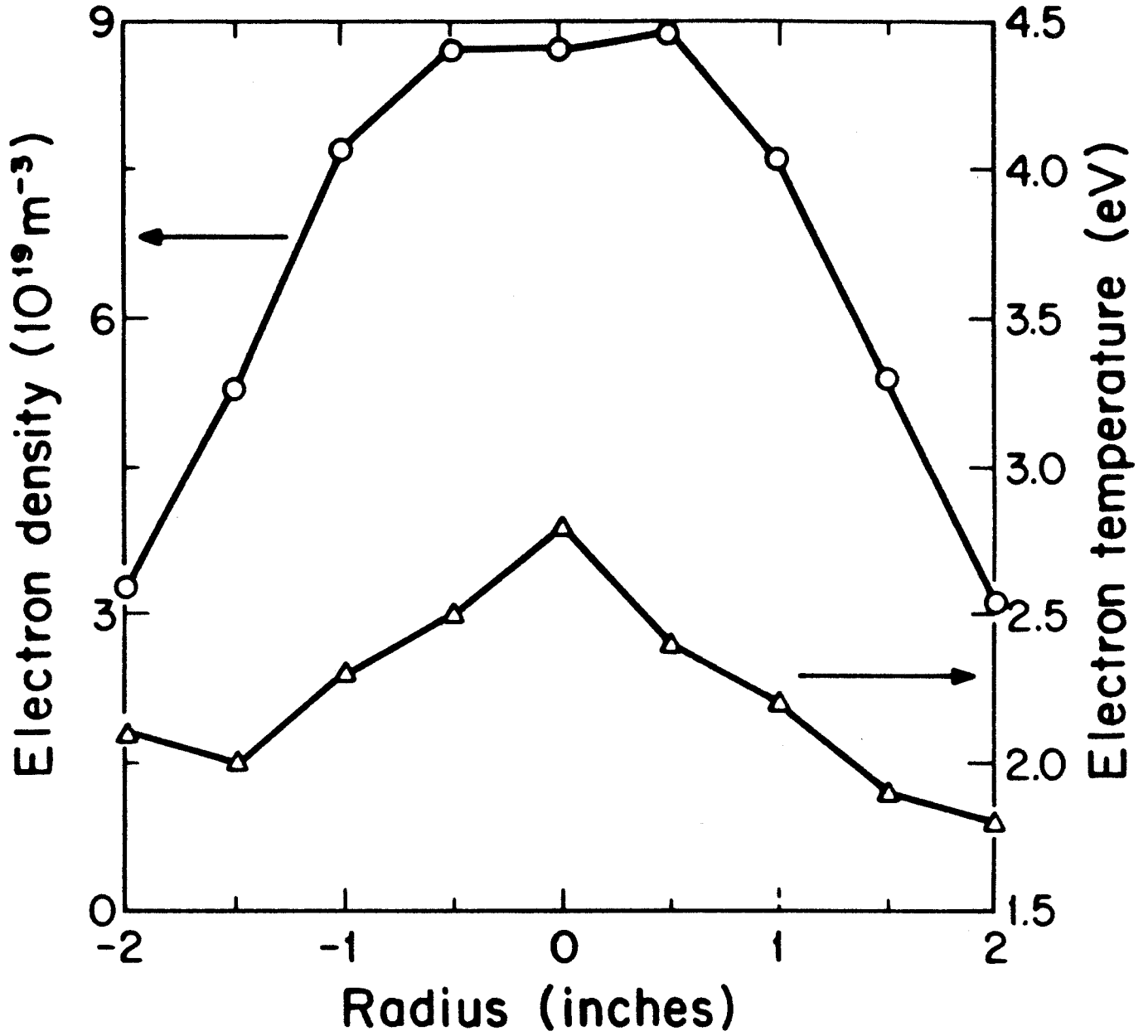


Figure 9. Deconvoluted H_{α} spectral-line for 20 kW of RF power and 1110 A of H.

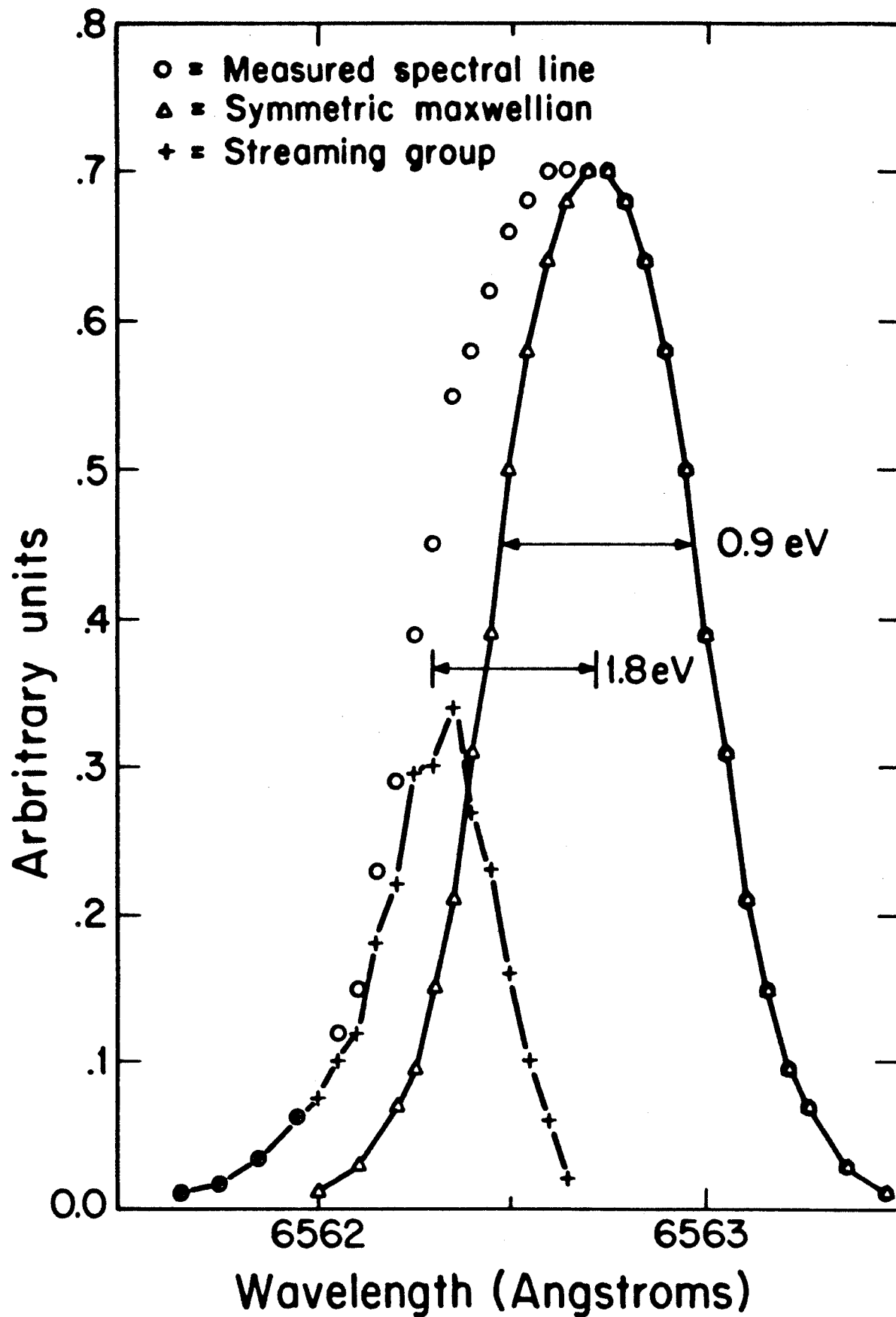


Figure 10. Average ion temperature vs. RF power for various hydrogen feed-rates.

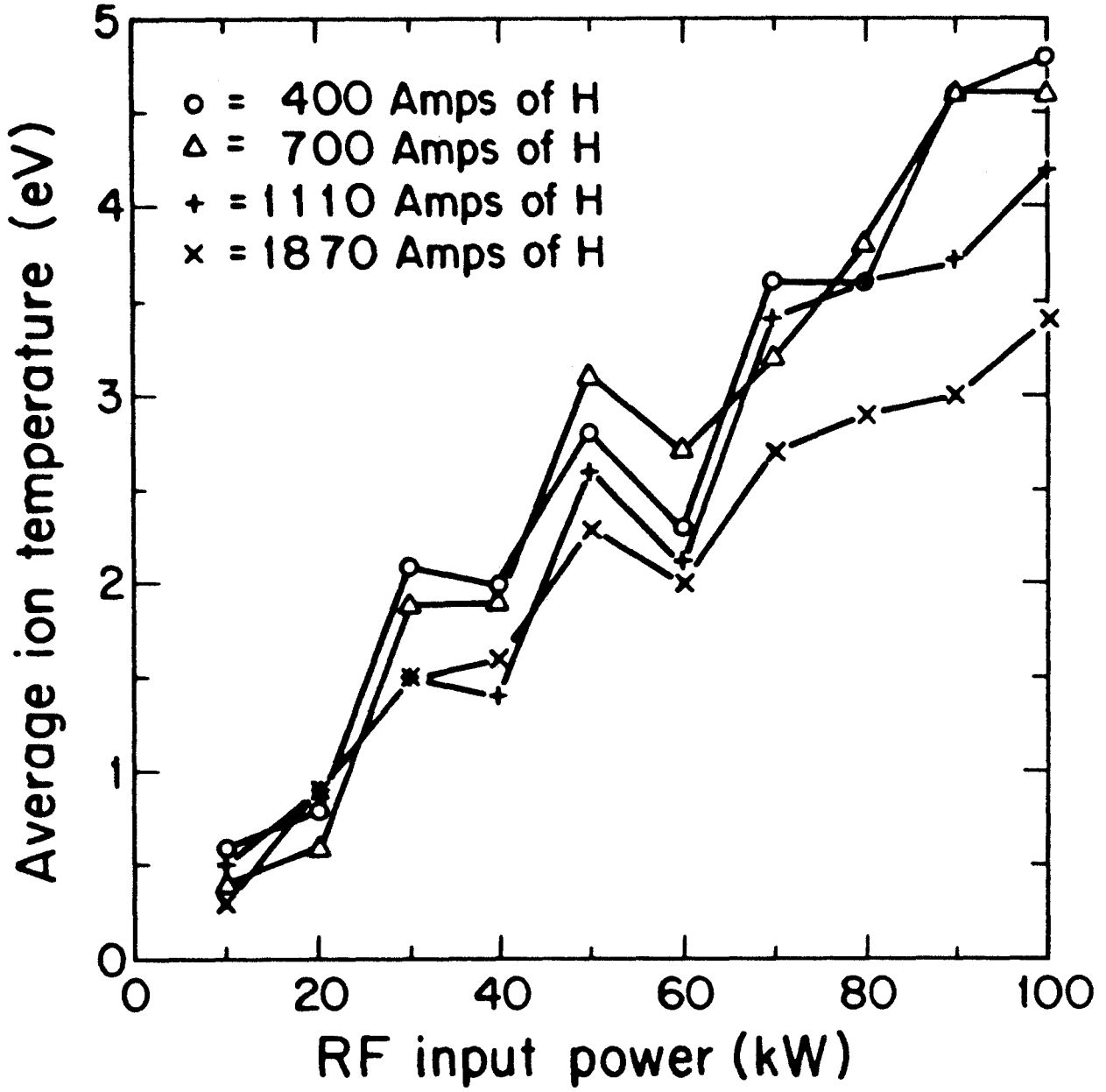


Figure 11. AC bridge for measuring change in thermistor resistance.

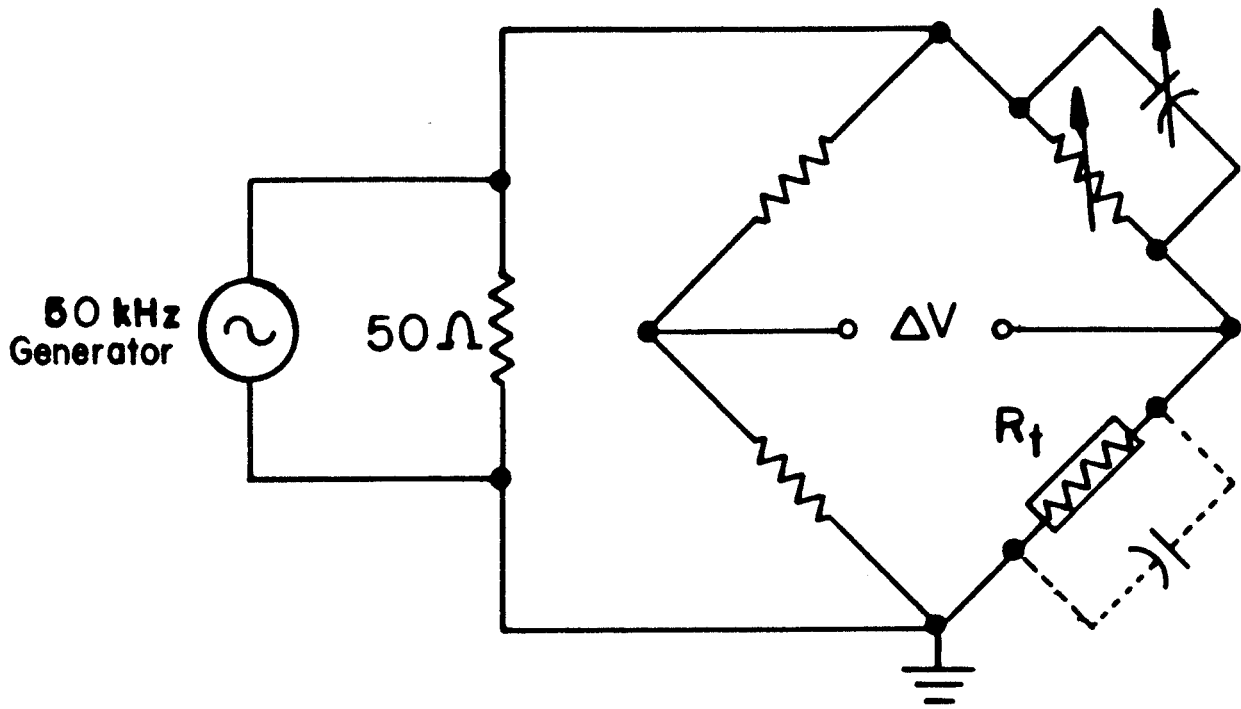


Figure 12. Theoretical and experimental plasma loading-resistance vs. RF power for 1570 A of H.

